Oxidation states and thermoelectric properties of BiCuSeO bulks fabricated under Bi or Se deficiencies in the nominal composition

Mamoru Ishizawa, Yuki Yasuzato, Hiroyuki Fujishiro, Tomoyuki Naito, Hirokazu Katsui, and Takashi Goto

Citation: Journal of Applied Physics **123**, 245104 (2018); doi: 10.1063/1.5034499
View online: https://doi.org/10.1063/1.5034499
View Table of Contents: http://aip.scitation.org/toc/jap/123/24
Published by the American Institute of Physics

Oxidation states and thermoelectric properties of BiCuSeO bulks fabricated under Bi or Se deficiencies in the nominal composition

Mamoru Ishizawa,[1] Yuki Yasuzato,[1,a)] Hiroyuki Fujishiro,[1,b)] Tomoyuki Naito,[1]
Hirokazu Katsui,[2] and Takashi Goto[2]
[1]*Faculty of Science and Engineering, Iwate University, Morioka 020-8551, Japan*
[2]*Institute for Materials Research, Tohoku University, Sendai 980-8577, Japan*

(Received 12 April 2018; accepted 5 June 2018; published online 25 June 2018)

We have fabricated the BiCuSeO bulks using raw materials with Bi or Se deficiencies in the nominal composition and investigated crystallographic, chemical compositional, and thermoelectric properties. Owing to the Bi or Se deficiencies in the starting composition, excessive elements and related compounds were deposited as impurity phases and the matrix phase is nearly the stoichiometric BiCuSeO phase. The electrical resistivity, $\rho(T)$, of the bulks decreases and thermoelectric power, $S(T)$, also decreases with increasing the contents of Bi or Se deficiencies in the starting composition in spite of the stoichiometric matrix phase. These results strongly suggest that, from the X-ray photoelectron spectroscopy measurements, the actual oxidation states of Bi and Cu deviate from the formal valences of stoichiometric $Bi^{3+}Cu^{1+}Se^{2-}O^{2-}$. The introduction of a small amount of Bi and Se vacancies is also suggested. As a result, mobile carriers are introduced and the ρ and S values are changed. The maximum thermoelectric dimensionless figure of merit of $ZT = 0.60$ was achieved at 773 K for the $Bi_{1-x}CuSeO$ samples ($x = 0.025$ and 0.05) in the starting composition. These results are in clear contrast with the reported results for the Cu deficiency bulks. Using these results, we propose charge valence equations and the origin of the carriers in the present BiCuSeO bulks and discuss the influence of created carriers on the thermoelectric properties. *Published by AIP Publishing.* https://doi.org/10.1063/1.5034499

I. INTRODUCTION

Oxide thermoelectric materials could be potential candidates in practical applications on the basis of their advantages over heavy metallic alloys in terms of chemical and thermal robustness, compared with conventional thermoelectric materials, such as Bi_2Te_3 and PbTe. The performance of thermoelectric materials can be written using the dimensionless figure of merit, ZT ($=S^2T/\rho\kappa$), and the thermoelectric power factor P ($=S^2/\rho$), where S is the Seebeck coefficient, T is the absolute temperature, ρ is the electrical resistivity, and κ is the thermal conductivity. However, the present potential of the oxide materials is relatively low.

Recently, n-type oxyselenides, BiCuSeO, have been paid considerable attention for a relatively higher thermoelectric performance from 700 to 1000 K.[1–13] This material crystallizes in a layered crystal structure that is composed of conductive $[Cu_2Se_2]^{2-}$ layers constituting a conduction pathway for carrier transport alternately stacked with insulating $[Bi_2O_2]^{2+}$ layers acting as a charge reservoir along the c-axis of the tetragonal unit cell, which is similar to layered cobaltites and iron-based superconductors.[2,3] For the enhancement of the thermoelectric properties, BiCuSeO showed an excellent charge transport behavior owing to the introduction of hole carriers by replacing Bi^{3+} with divalent alkaline-earth ions such as Sr^{2+}, Ba^{2+}, Ca^{2+}, and Pb^{2+} in the insulating $[Bi_2O_2]^{2+}$ layer.[8,9,13] In the $[Cu_2Se_2]^{2-}$ layer, the replacement of the Se^{2-} site with the isovalent Te^{2-} also enhances the thermoelectric properties owing to the opening of a small gap in the electronic structure.[14] The hole doping also induces point defect scattering, which reduces the thermal conductivity and results in the ZT enhancement. The highest ZT of 1.4 was achieved at 923 K for the $Bi_{0.875}Ba_{0.125}CuSeO$ sample to date,[15] which is higher than that for other n-type thermoelectric oxides such as $SrTi_{0.8}Nb_{0.2}O_3$ ($ZT = 0.37$ at 1000 K),[16] $Zn_{0.98}Al_{0.02}O$ ($ZT = 0.30$ at 1273 K),[17] and $In_{2-x}Ge_xO_3$ ($ZT = 0.45$ at 1273 K).[18]

The deficiency of Cu^{1+} was also investigated by the introduction of hole carriers. $BiCu_{1-x}SeO$,[19,20] $LaCu_{1-x}SO$,[21,22] and BaCu*Ch*F (*Ch*: chalcogen) systems[23] introduce hole carriers into the charge conductive selenide $(Cu_2Se_2)^{2-}$ layers and decrease the resistivity. In these samples, the Cu deficiencies exist actually and the lattice parameter monotonically changes depending on the Cu deficiencies.[19] However, there are no reports for the thermoelectric properties of the BiCuSeO samples with Bi or Se deficiencies.

In this study, we investigated the influence of Bi or Se deficiencies in the starting composition on thermoelectric properties in the BiCuSeO system. The impurity phases were identified, and the lattice parameters and the chemical composition in the matrix phase were in clear contrast with the reported Cu deficient samples.[19] Using the results of X-ray photoelectron spectroscopy (XPS) and standard defect theory, we propose charge valence equations and the origin of the carriers in the present BiCuSeO bulks and discuss the influence of created carriers on the thermoelectric properties.

[a)]Present address: Department of Applied Physics, Graduate School of Engineering, Tohoku University, Sendai 980-8579, Japan.
[b)]Author to whom correspondence should be addressed: fujishiro@iwate-u.ac.jp

II. EXPERIMENTAL PROCEDURE

The BiCuSeO materials were fabricated using Bi (99.9%) and Bi_2O_3 (99.9%), Cu (99.9%), and Se (99.9%) fine powders as raw materials. For the Bi deficient samples for the nominal composition, these were weighed with the ratio of Bi:Cu:Se = 1–x:1:1 and mixed in an Ar atmosphere. For the Se deficient samples for the nominal composition, these were weighed with the ratio of Bi:Cu:Se = 1:1:1–y and mixed in an Ar atmosphere. After the mixed raw materials were evacuated and sealed in a quartz tube, they were heated at 973 K for 12 h and then furnace-cooled. The obtained precursor was pulverized and mixed in air for 0.5 h by an automatic mortar. The powders were sintered using the spark plasma sintering (SPS) apparatus (NJS, LABOX-110C) under a uniaxial pressure of 40 MPa at about 973 K for 10 min in vacuum. The mass density of the obtained pellets (10 mm in diameter and 9 mm in thickness) was higher than 93% of the ideal density. We denoted the nominal composition of the fabricated materials, as $Bi_{1-x}CuSeO$ and $BiCuSe_{1-y}O$, respectively, which are not the measured composition for the bulk.

Powder X-ray diffraction (XRD) measurements were performed (Rigaku, Multi Flex) at room temperature using Cu $K\alpha$ radiation to confirm the impurity phase in the sintered bulks and to decide the lattice constants using Rietveld refinement.[24] The microstructure and chemical composition of sintered bulks were analyzed by scanning electron microscopy (SEM) and an electron probe micro-analyzer with a field emission gun (FE-EPMA). The sintered pellet fabricated by SPS was sliced perpendicular to the uniaxial pressure direction and rectangular-shaped bars were prepared and the thermoelectric properties were measured. We confirmed that the thermoelectric properties were independent of the cutting direction of the bar, although the crystal structure of BiCuSeO is anisotropic. The electrical resistivity, $\rho(T)$, and Seebeck coefficient, $S(T)$, were simultaneously measured in the temperature range from 300 to 773 K using an automated measuring system (Ozawa Science RZ2001i) and the thermoelectric power factor, $P = S^2/\rho$, was calculated. The thermal conductivity $\kappa(T)$ was estimated from 300 to 773 K using the relationship $\kappa = D\alpha C$, where α is the thermal diffusivity, which was measured by a laser flash method (Ulvac-Riko TC-7000), C is the specific heat of the $x = y = 0$ sample, which was measured by the laser flash method, and D is the mass density, which was measured by the Archimedes method. A dimensionless figure of merit, $ZT = S^2T/\rho\kappa$, was estimated using these values, in which the involved uncertainty is about 20%. X-ray photoelectron spectroscopy (XPS; Ulvac Phi PHI5600) was measured for the samples after the Ar sputtering by 20 μm in depth. Hall effect experiments were carried out by the five-terminal method at room temperature to determine the carrier concentration, p, and Hall mobility, μ, which was calculated by $\mu = R_H/\rho$ (R_H = Hall coefficient).

III. RESULTS AND DISCUSSION

A. Crystallographic properties

Figures 1(a) and 1(b) show the magnification of XRD patterns of the $Bi_{1-x}CuSeO$ and $BiCuSe_{1-y}O$ samples around the main peak of (101) diffraction, respectively. Note again that the notation of "$Bi_{1-x}CuSeO$" and "$BiCuSe_{1-y}O$" is not the measured composition, but the nominal composition of the fabricated materials. For both systems, the matrix phase was confirmed to be a BiCuSeO phase by XRD measurements, in which the peak angle of the (101) diffraction does not shift for the x or y values. However, for the Bi deficient samples shown in Fig. 1(a), the CuSe impurity phase can be seen and increases with increasing x in the nominal composition. For the Se deficient system, as shown in Fig. 1(b), the peaks of Bi and Bi_2O_3, both of which are raw materials, increase with increasing y in the nominal composition, which result from the shortage of the Se atoms in the starting materials. Although the precipitation of the Cu_2Se phase is expected in this case, the Cu_2Se phase was not detected by XRD. These results suggest that a stoichiometric BiCuSeO phase was obtained as a matrix phase and, as a result, the expected impurity phases were detected, which increase with increasing Bi or Se deficiencies in the nominal composition. The details of the issue are discussed later.

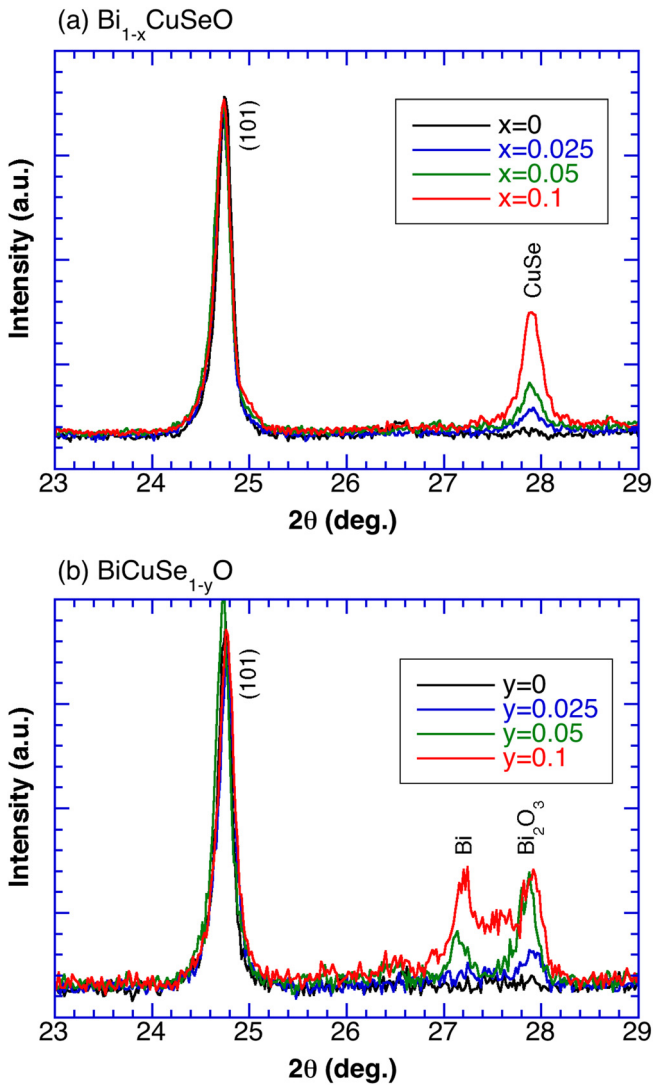

FIG. 1. XRD patterns of the (a) $Bi_{1-x}CuSeO$ and (b) $BiCuSe_{1-y}O$ samples around the (101) diffraction. The notation of $Bi_{1-x}CuSeO$ and $BiCuSe_{1-y}O$ is not the realistic composition, but the nominal composition of the fabricated materials.

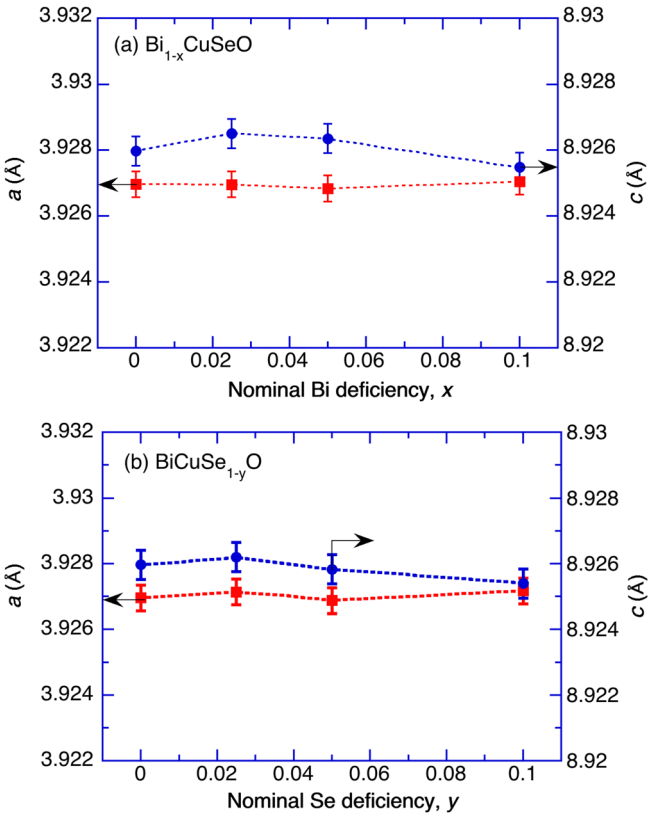

FIG. 2. The lattice parameters along the *a*-axis and *c*-axis of the (a) $Bi_{1-x}CuSeO$ and (b) $BiCuSe_{1-y}O$ samples, as a function of Bi or Se deficiency in the nominal composition.

Figures 2(a) and 2(b) show the estimated lattice parameters of the $Bi_{1-x}CuSeO$ and $BiCuSe_{1-y}O$ samples, respectively, as a function of Bi or Se deficiency in the nominal composition. For both systems, the BiCuSeO matrix phase can be fitted by the RIETAN program[24] within $R_{wp} = 5\%$ and $s = 1.5$. The lattice parameter in the *ab*-plane is nearly the constant, independent of the x or y value. The lattice parameter along the *c*-axis is the constant until $x = y = 0.05$, but is seemed to decrease slightly for the $x = y = 0.1$ samples. It should be noticed that the results of the lattice parameter are in clear contrast with those for the reported Cu deficient samples,[19] in which the *a*-axis and *c*-axis lattice parameters of the $BiCu_{0.9}SeO$ sample shrink about 0.076% and 0.22%, respectively. The difference of the results with this study may essentially come from the difference in the deficiency site or may come from the difference of the fabrication process.

Figure 3(a) shows the backscattered electron composition (BEC) images of the BiCuSeO sample without any deficiency in the nominal composition. Black regions are voids and a small amount of dark gray regions shown by blue arrows are Bi_2O_3. Figures 3(b) and 3(c) show the BEC images of the $Bi_{1-x}CuSeO$ samples ($x = 0.05$ and 0.1) in the nominal composition. Tables I and II show the ratio of each element for the matrix phase in the $Bi_{1-x}CuSeO$ and $BiCuSe_{1-y}O$ samples, respectively, in which the total of the ratios is normalized to be 4.00. The EPMA measurements were performed at 3 points for each sample and each phase and then averaged. The element composition ratio in the

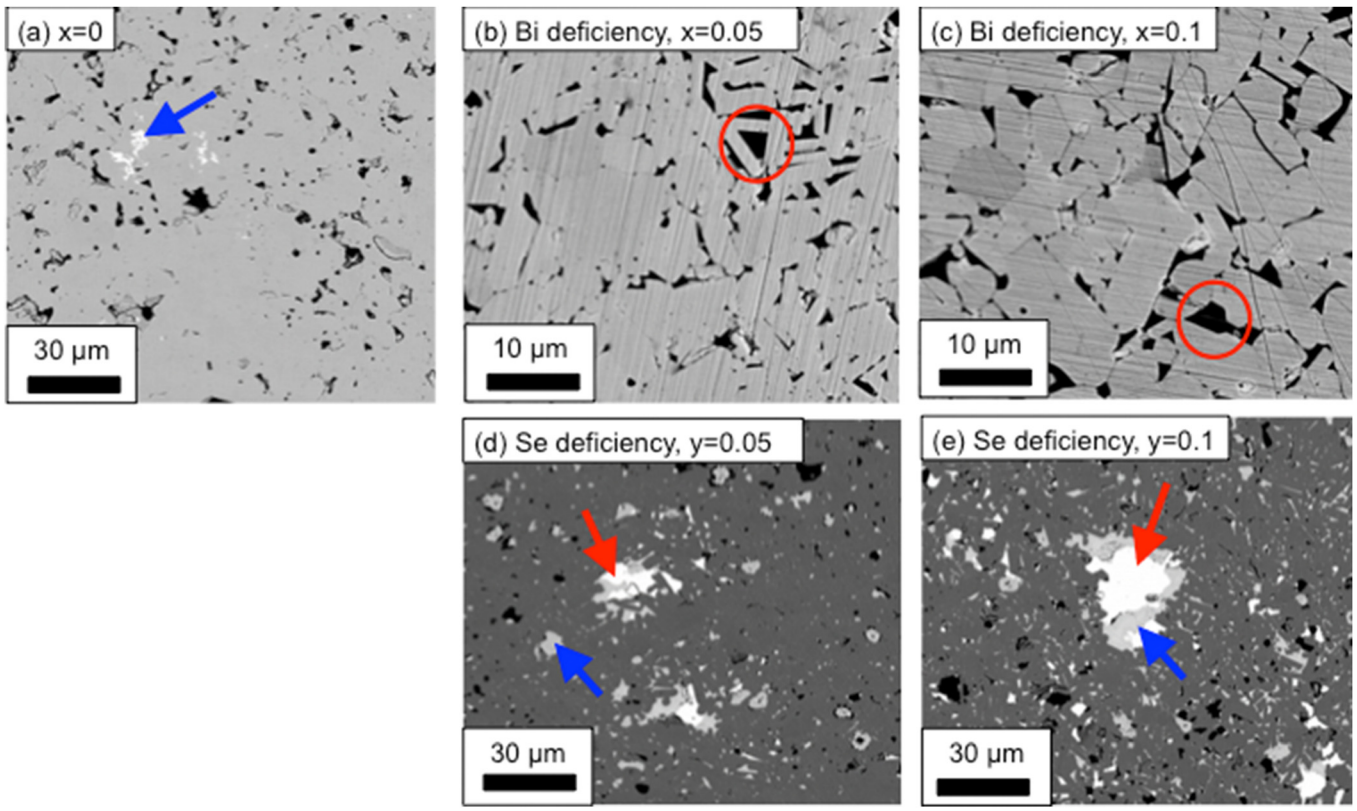

FIG. 3. Backscattered electron composition (BEC) images of the (a) BiCuSeO sample without any deficiency in the nominal composition, $Bi_{1-x}CuSeO$ samples [(b) $x = 0.05$ and (c) $x = 0.1$] and $BiCuSe_{1-y}O$ samples [(d) $y = 0.05$ and (e) $y = 0.1$]. In (b) and (c), the black regions are confirmed to be CuSe. In (a), (d), and (e), the bright regions (red arrow) and dark gray regions (blue arrow) are, respectively, Bi and Bi_2O_3 raw materials.

TABLE I. Estimated atomic ratios of Bi:Cu:Se:O for the matrix phase in the $Bi_{1-x}CuSeO$ samples by EPMA, in which the total of the ratios is normalized to be 4.00.

	Bi	Cu	Se	O	Total
$x = 0$	1.02	1.11	0.98	0.88	4.00
$x = 0.025$	1.04	1.07	0.99	0.90	4.00
$x = 0.05$	1.04	1.08	0.98	0.89	4.00
$x = 0.1$	1.04	1.09	0.99	0.88	4.00

matrix phase is nearly Bi: Cu:Se:O = 1:1:1:1, which is independent of the x or y value. These results suggest that the $Bi_{1-x}CuSeO$ materials were fabricated according to the following equation, in which the matrix phase is nearly stoichiometric in spite of the introduction of the Bi deficiency into the nominal composition and support the results of Fig. 2(a)

$$\frac{1}{3}(1-3x)\mathrm{Bi} + \frac{1}{3}\mathrm{Bi_2O_3} + \mathrm{Cu} + \mathrm{Se} \rightarrow (1-x)\mathrm{BiCuSeO} + x\mathrm{CuSe} + x\mathrm{O}. \quad (1)$$

In Figs. 3(b) and 3(c) for the $Bi_{1-x}CuSeO$ samples, the contents and size of the black region marked in a red circle, which was confirmed to be the CuSe phase by EPMA, increase with increasing x. These results support the XRD results shown in Fig. 1(a).

Figures 3(d) and 3(e), respectively, show the BEC images of the $BiCuSe_{1-y}O$ samples ($y = 0.05$ and 0.1) in the nominal composition. The contents of the bright regions shown by red arrows and the dark grey regions shown by blue arrows increase with increasing y. These phases were identified as Bi and Bi_2O_3 raw materials, respectively. The black region in these figures was identified as Cu_2Se by EPMA, but cannot be detected by XRD. These results suggest that the $BiCuSe_{1-y}O$ materials were fabricated according to the following equation, in which the matrix phase is nearly stoichiometric in spite of the introduction of the Se deficiency into the nominal composition and support the results of Fig. 2(b)

$$\frac{1}{3}\mathrm{Bi} + \frac{1}{3}\mathrm{Bi_2O_3} + \mathrm{Cu} + (1-y)\mathrm{Se} \rightarrow (1-2y)\mathrm{BiCuSeO} + y\mathrm{Cu_2Se} + \frac{2}{3}y\mathrm{Bi_2O_3} + \frac{2}{3}y\mathrm{Bi}. \quad (2)$$

B. Thermoelectric properties

Figures 4(a) and 4(b) show the temperature dependence of the electrical resistivity, $\rho(T)$, of the $Bi_{1-x}CuSeO$ and $BiCuSe_{1-y}O$ samples, respectively. In Fig. 4(a), the $\rho(T)$ of the

TABLE II. Estimated atomic ratios for the matrix phase in the $BiCuSe_{1-y}O$ samples by EPMA, in which the total of the ratios is normalized to be 4.00.

	Bi	Cu	Se	O	Total
$y = 0$	1.02	1.11	0.98	0.88	4.00
$y = 0.025$	1.02	1.11	0.99	0.88	4.00
$y = 0.05$	1.01	1.13	1.00	0.87	4.00
$y = 0.1$	1.02	1.12	0.98	0.88	4.00

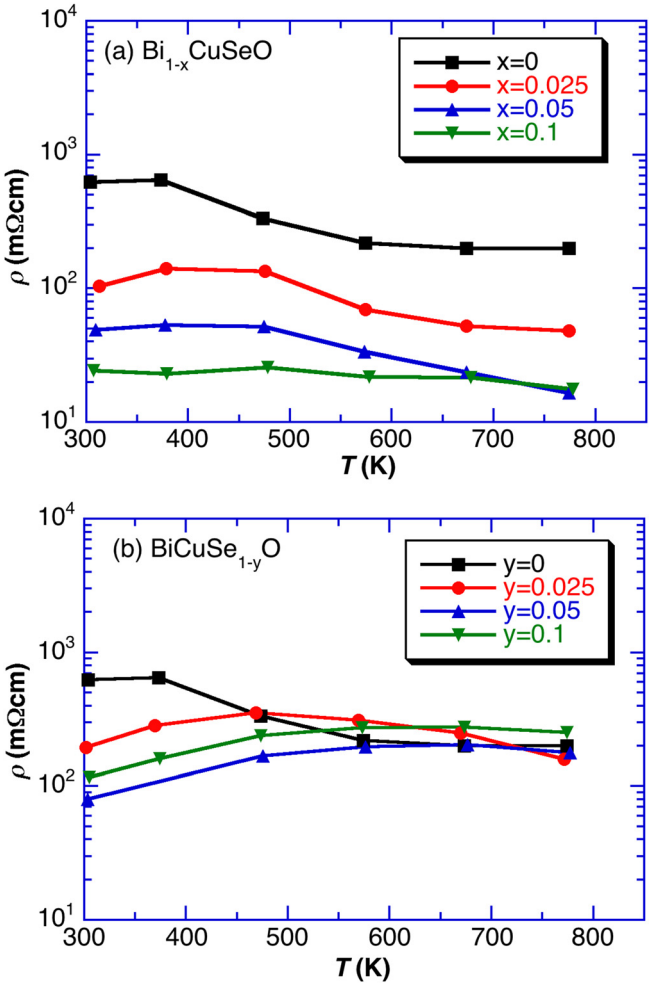

FIG. 4. Temperature dependence of the electrical resistivity, $\rho(T)$, of the (a) $Bi_{1-x}CuSeO$ and (b) $BiCuSe_{1-y}O$ samples in the nominal composition.

$Bi_{1-x}CuSeO$ samples decreases with increasing x. The reduction in $\rho(T)$ is simply understood from the introduction of hole carriers. On the other hand, the behavior of the $\rho(T)$ in the $BiCuSe_{1-y}O$ samples as a function of the y value shown in Fig. 4(b) is fairly different with that of $Bi_{1-x}CuSeO$ samples; the $\rho(T)$ value decreased for the y value up to 0.05 and then slightly increased for the $y = 0.1$ sample, and the $\rho(T)$ value at high temperatures is independent of the y value. The detailed discussion about the different behaviors between both systems and the origin of the created carriers are shown in 3.3.

Figures 5(a) and 5(b) show the temperature dependence of the Seebeck coefficient, $S(T)$, for the $Bi_{1-x}CuSeO$ and $BiCuSe_{1-y}O$ samples above 300 K, respectively. In Fig. 5(a), the S value for the $x = 0$ sample exceeds $+400\,\mu$V/K, which shows a p-type material, and decreases with increasing x. For the $BiCuSe_{1-y}O$ samples shown in Fig. 5(b), the S value slightly decreases with increasing y and the $S(T)$ value at high temperatures is independent of the y value. These results strongly suggested that the $S(T)$ value is closely related to the $\rho(T)$ value.

Figures 6(a) and 6(b) show the temperature dependence of the thermoelectric power factor, $P(T) = S^2/\rho$, for the $Bi_{1-x}CuSeO$ and $BiCuSe_{1-y}O$ samples above 300 K, respectively. In the $Bi_{1-x}CuSeO$ samples, the $P(T)$ value increases

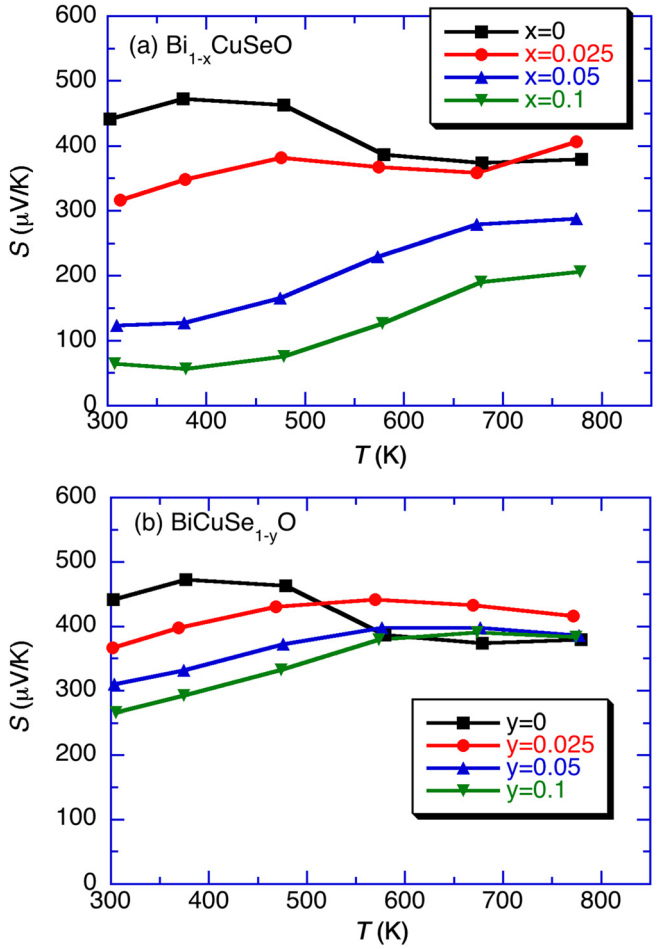

FIG. 5. Temperature dependence of the Seebeck coefficient, $S(T)$, of the (a) $Bi_{1-x}CuSeO$ and (b) $BiCuSe_{1-y}O$ samples in the nominal composition.

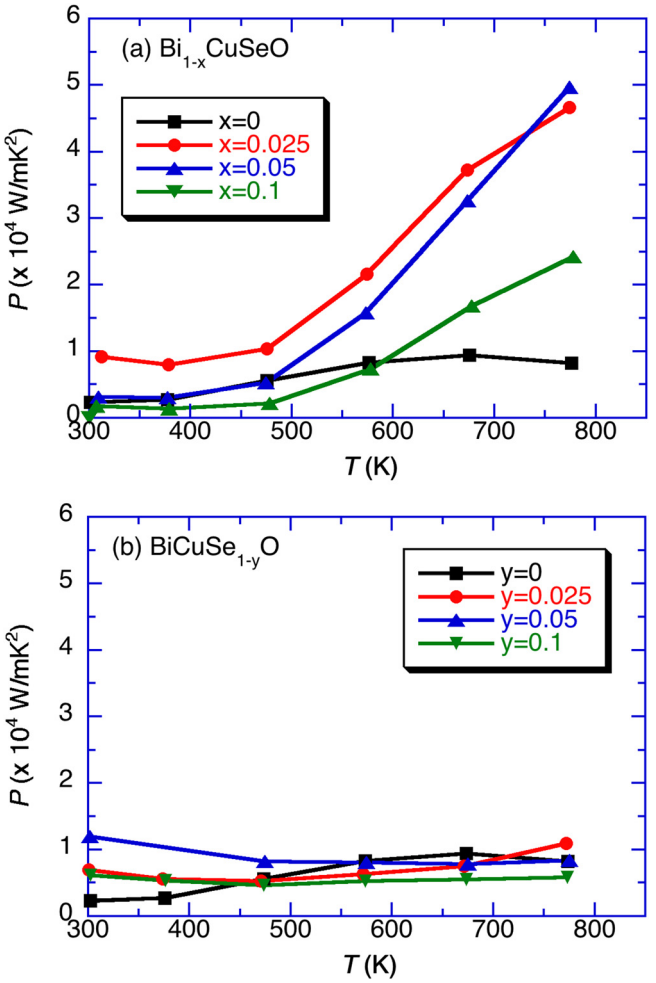

FIG. 6. Temperature dependence of the thermoelectric power factor, $P(T) = S^2/\rho$, of the (a) $Bi_{1-x}CuSeO$ and (b) $BiCuSe_{1-y}O$ samples in the nominal composition.

with increasing T and that at high temperatures takes a maximum for the $x = 0.025$ and 0.05 samples and then slightly decreases for the $x = 0.1$ sample. The highest P value of 5.0×10^{-4} W m^{-1} K^{-2} was achieved for the $Bi_{0.95}CuSeO$ sample at 773 K, which is about five times larger than that for the $x = 0$ sample. On the other hand, for the $BiCuSe_{1-y}O$ samples shown in Fig. 6(b), the $P(T)$ value is fairly low and independent of the y value, which comes from the small y dependence of $\rho(T)$ and $S(T)$ values.

Figures 7(a) and 7(b) show the temperature dependence of the thermal conductivity, $\kappa(T)$, for the $Bi_{1-x}CuSeO$ and $BiCuSe_{1-y}O$ samples, respectively. $\kappa(T)$ hardly depends on the x and y values at the entire temperature range. This result originates from the dominant phonon scattering due to the intrinsic lattice vibration and suggests that the matrix phase is nearly the stoichiometric composition. In the $BiCu_{1-x}SeO$ and $Bi_{1-x}Ca_xCuSeO$ systems, $\kappa(T)$ decreases with increasing x, which indicates that the phonons are mainly scattered by the crystal defects and inhomogeneity.[13,19]

Figures 8(a) and 8(b) show the temperature dependence of the thermoelectric figure of merit, $ZT(T)$, for the $Bi_{1-x}CuSeO$ and $BiCuSe_{1-y}O$ samples, respectively. The ZT values of all the samples increased with increasing temperature. In Fig. 8(a), the $ZT(T)$ value takes a maximum for the $Bi_{1-x}CuSeO$ samples at $x = 0.025$ and 0.05 and then decreased with increasing x, which is closely related to the thermoelectric power factor $P(T)$, because the $\kappa(T)$ is independent of x. The maximum ZT of 0.60 was achieved at 773 K for the $Bi_{1-x}SrCuSeO$ bulks ($x = 0.025$ and 0.05). On the other hand, for the $BiCuSe_{1-y}O$ samples, shown in Fig. 8(b), the $ZT(T)$ values are quite small and are independent of the y value, which is in clear contrast with those of the $Bi_{1-x}CuSeO$ samples.

Figure 9(a) shows the carrier concentration, p, and carrier mobility, μ, of the $Bi_{1-x}CuSeO$ samples, as a function of the Bi deficiency, x, in the nominal composition, both of which were estimated by the Hall effect measurement. In the figure, the error bars of the p values of 18% come from the difference of positive and negative Hall voltages and those of the μ values of 30% come from both the measurement errors of the sample size and the resistivity. The carrier concentration, p, increases and the carrier mobility, μ, monotonically decreases with increasing x. These results originate from the introduction of the hole carriers and the phonon scattering owing to the increase in the impurity phases and introduced carriers, both of which are reasonable characteristics. In general, the electrical resistivity, ρ, and carrier mobility, μ, in a material can be represented as $\rho = m^*/pe^2\tau$ and $\mu = e\tau/m^*$,

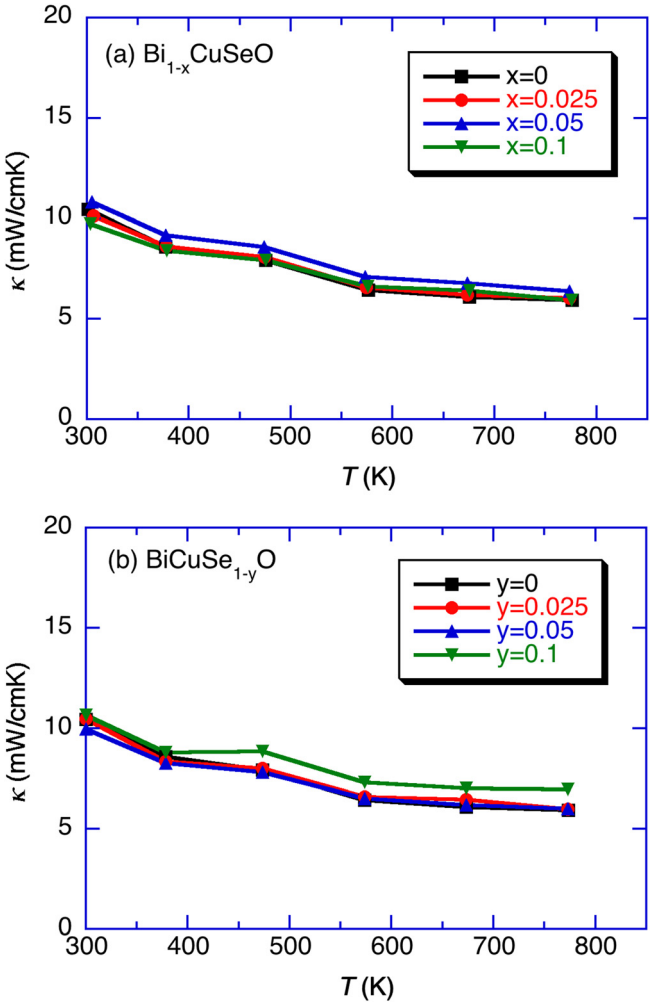

FIG. 7. Temperature dependence of the thermal conductivity, $\kappa(T)$, of the (a) $Bi_{1-x}CuSeO$ and (b) $BiCuSe_{1-y}O$ samples in the nominal composition.

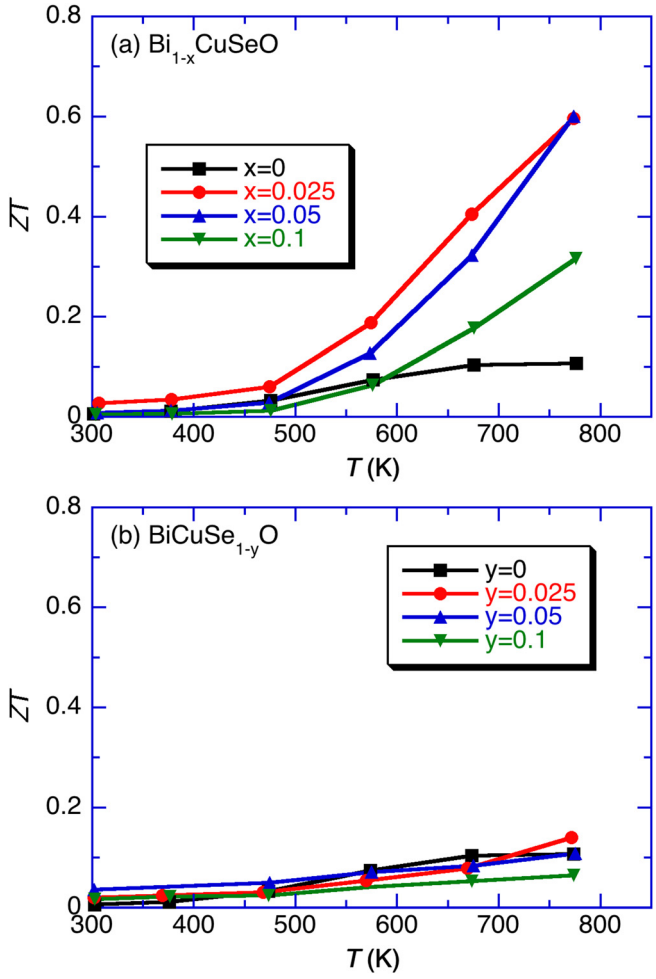

FIG. 8. Temperature dependence of the thermoelectric figure of merit, $ZT(T)$, of the (a) $Bi_{1-x}CuSeO$ and (b) $BiCuSe_{1-y}O$ samples in the nominal composition.

respectively (m^*: effective mass of carriers, τ: mean free time, e: unit charge). In these equations, the ρ value is inversely proportional to both p and τ values, and the μ value is proportional to the τ value. Since the τ value decreases with increasing the contents of impurities and carriers, in general, the ρ value shown in Fig. 4(a) and the μ value shown in Fig. 9(a) of the $Bi_{1-x}CuSeO$ samples are reasonable. On the other hand, these characteristics are in clear contrast to those for the $BiCuSe_{1-y}O$ samples. Figure 9(b) shows the p and μ values of the $BiCuSe_{1-y}O$ samples, as a function of the Se deficiency, y, in the nominal composition. The p values slightly increase up to $y = 0.05$, but decrease for the $y = 0.1$ sample. The μ values seem to show the similar y dependence to the p values. However, these results cannot be systematically explained as a function of the y value, which may result from the complicated contribution from p and τ values.

C. XPS results and proposed charge valence equations

To explain these experimental results, we carried out XPS spectroscopy. We proposed the charge valence equations and the origin of the carriers in the present BiCuSeO bulks fabricated from starting raw materials with intentionally introduced Bi or Se deficiencies.

Figures 10(a)–10(c), respectively, show the binding energy spectrum of Bi, Cu, and Se measured by XPS for the non-doped BiCuSeO sample at room temperature. Figures 10(d)–10(f), respectively, show the same binding energy spectrum for the $Bi_{0.9}CuSeO$ sample. Figures 10(g)–10(i), respectively, also show the same binding energy spectrum for the $BiCuSe_{0.9}O$ sample. In the figures, the energy separation curves, which were obtained using Gaussian functions, are also shown. The binding energies of these valence states for each element shown in Fig. 10 are fairly consistent with those of the reported values.[1,25] For the non-doped BiCuSeO sample, the oxidation state of Bi is mainly Bi^{3+} and a small amount of Bi^{2+} and Bi^{4+} co-exist [Fig. 10(a)]. The oxidation state of Cu is mainly Cu^{1+} and a small amount of Cu^{2+} co-exists [Fig. 10(b)]. The oxidation state of Se, in which the binding energy difference between the spin-orbit doublets of $3d^{3/2}$ and $3d^{5/2}$ in Se is known to be small, is confirmed to be Se^{2-} [Fig. 10(c)]. The peak can be separated by two Gaussian peaks, which may come from the difference of the element bonded to Se.[25,26] The ideal oxidation states of the elements in BiCuSeO have been assumed to be Bi^{3+}, Cu^{1+}, $Se^{2,-}$ and O^{2-}, based on the requirement of the overall

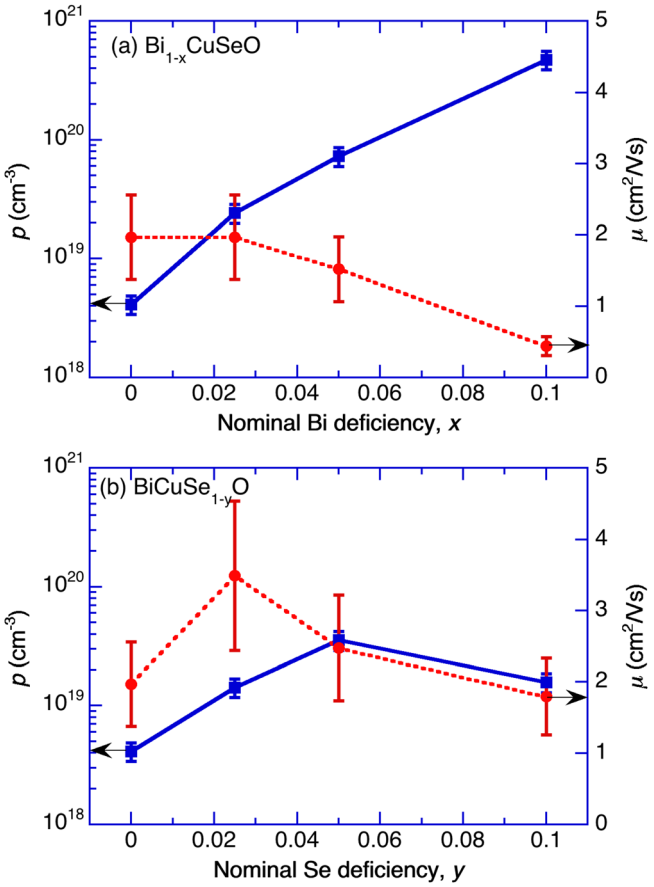

FIG. 9. Carrier concentration, p, and carrier mobility, μ, of the (a) $Bi_{1-x}CuSeO$ and (b) $BiCuSe_{1-y}O$ samples, as a function of the Bi deficiency, x, and the Se deficiency, y, in the nominal composition, respectively. These values were estimated by the Hall effect measurement.

charge neutrality.[19,27] Apparently, BiCuSeO is not a typical ionic compound and the oxidation state of each element must not be so explicitly defined. In an ideal stoichiometric composition and standard oxidation state of each element, non-doped BiCuSeO should be an insulator without any charge carriers. However, the actual non-doped BiCuSeO has moderate p-type conductivity. This may come from the intrinsic defects such as ion vacancies, interstitials, and anti-sites, which are the main contributions to the carriers by ionizations.

For the $Bi_{0.9}CuSeO$ sample, the oxidation state of Bi was entirely the Bi^{3+} [Fig. 10(d)], which is in clear contrast with that of the non-doped BiCuSeO sample. Based on the standard defect theory, hole carriers are introduced into the matrix phase by the increase in the Bi vacancy (V_{Bi}^{-}), which can accept electrons at most from the valence band maximum in principles.[28,29] In this case, the following charge valence equation is assumed and hole carriers are introduced into the $[Bi_2O_2]^{2+}$ insulating layers:

$$2Bi_{1-x}CuSeO = \left(Bi^{3+}_{2(1-x)}O^{2-}_{2}\right)^{2(1-3x)+} + \left(Cu^{1+}_{2}Se^{2-}_{2}\right)^{2-} + 2xV^{-}_{Bi} + 8xh^{+}, \quad (3)$$

where V_{Bi}^{-} is a Bi vacancy and h^{+} is a hole. It is likely to say that the reduction of $\rho(T)$ of the $Bi_{1-x}CuSeO$ with increasing x, as shown in Fig. 4(a), comes from the increase in the Bi vacancies in the matrix phase. In Fig. 2(a), we found the very small shrink of the c-axis lattice constant for the $Bi_{1-x}CuSeO$ samples ($x > 0.05$), which may closely relate to the introduction of Bi vacancies into the matrix phase. In the mixed valence of Cu, the ratio of Cu^{2+}/Cu^{1+} slightly increased from 0.073 for the non-doped BiCuSeO to 0.149 for the $Bi_{0.9}CuSeO$ [Fig. 10(e)]. The increase in the Cu^{2+} was also confirmed for the Ca-doped BiCuSeO, in which hole carriers were introduced and the $\rho(T)$ decreased with increasing Ca doping.[26] The change of the Cu oxidation state from +1 to +2 introduces donors and donates electrons to the conduction band minimum, which may compensate the hole carriers. However, the decrease in $\rho(T)$ in Fig. 2(a) and the increase in the p value in Fig. 9(a) strongly suggest that the introduction of acceptors due to the Bi vacancies fairly overcomes the donors due to the Cu oxidation with the increasing x.

For the $BiCuSe_{1-y}O$ samples, the XPS spectra of Bi, Cu, and Se, as shown in Figs. 10(g) to 10(i), hardly change largely, compared with those of the non-doped BiCuSeO sample, which are in clear contrast to those of the $Bi_{1-x}CuSeO$ sample, although the electrical characteristics change moderately. Figure 11 shows the ratios of Bi^{2+}/Bi^{3+} and Bi^{4+}/Bi^{3+} in the XPS spectra for the $BiCuSe_{1-y}O$ samples, as a function of the Se deficiency, y, in the nominal composition, which are extracted from Figs. 10(a) and 10(g). Both ratios took a minimum for the $y = 0.05$ sample and then increase for the $y = 0.1$ sample. These y dependences show a similar trend to the electrical resistivity shown in Fig. 4(b) and the reversal trend as the hole concentration shown in Fig. 9(b). These results suggest that the decrease in the Bi^{2+} and Bi^{4+} contents is closely related to the carrier concentration. These tendencies are also consistent with the case of $Bi_{1-x}CuSeO$ samples, in which the Bi^{2+} and Bi^{4+} vanish in the $Bi_{0.9}CuSeO$ sample and electrical resistivity is fairly reduced due to the carrier doping.

In Fig. 2(b), a very small shrink in the c-axis lattice constant can be also seen for the $BiCuSe_{1-y}O$ samples ($y > 0.05$). This may result from the introduction of a very small amount of actual Se vacancies into the matrix phase, in which the following charge valance equation is assumed and electrons are introduced into the $[Cu_2Se_2]^{2-}$ conducting layers

$$2BiCuSe_{1-y}O = \left(Bi^{3+}_{2}O^{2-}_{2}\right)^{2+} + \left(Cu^{1+}_{2}Se^{2-}_{2(1-y)}\right)^{2(1-2y)-} + 2yV^{+}_{Se} + 6ye^{-}, \quad (4)$$

where V_{Se}^{+} is a Se vacancy and e^{-} is an electron. In this case, the created electrons are compensated by the intrinsic hole carriers and the electrical resistivity should be enhanced. However, a small amount of Bi vacancies, which introduce the acceptor, may also be created in the Se deficient samples at the same time. At present, we cannot exactly explain the relationship between the defect formation and the carrier creation for the $BiCuSe_{1-y}O$ sample. We limit to present the experimental results and a simple discussion

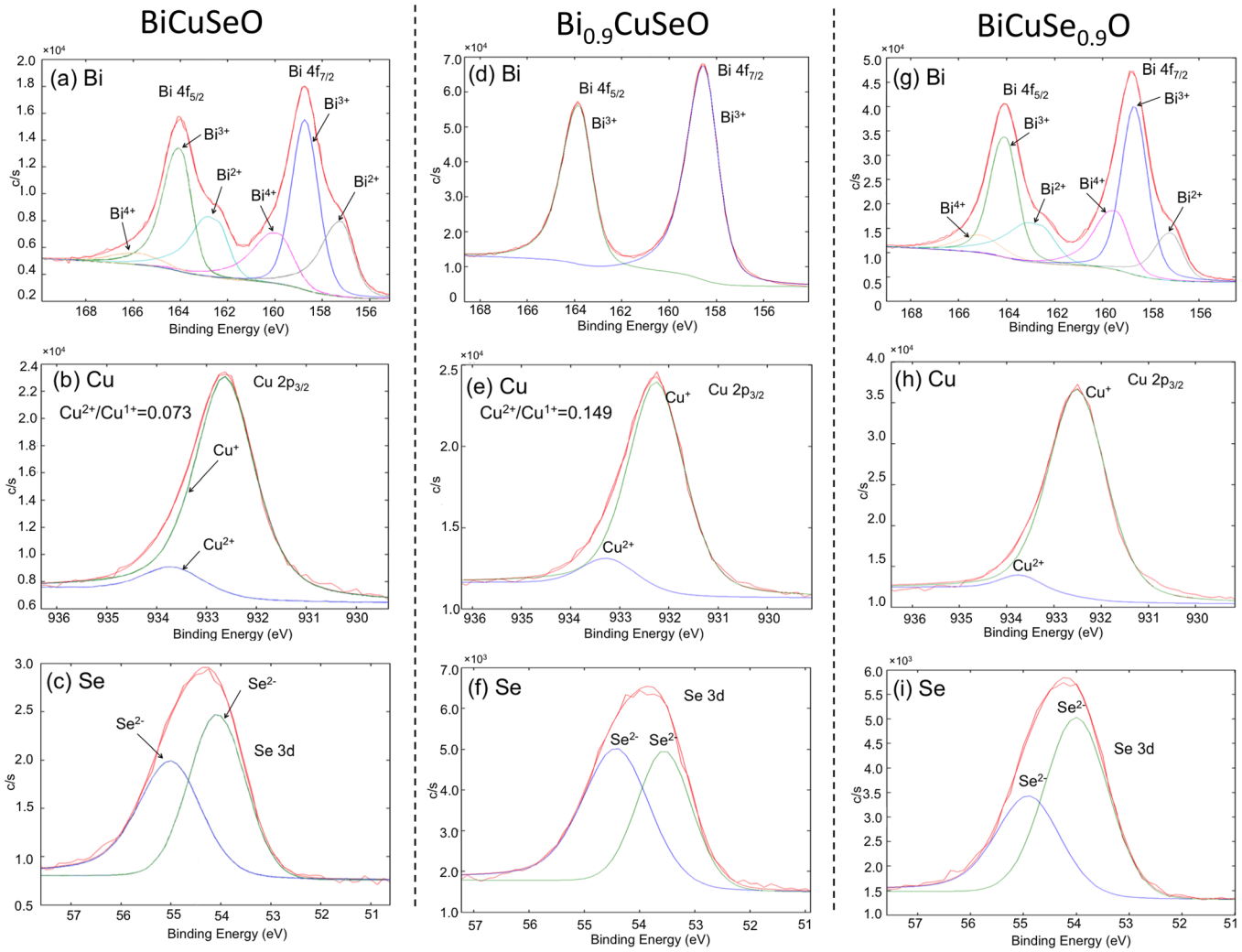

FIG. 10. XPS spectra at the binding energy for Bi, Cu, and Se of non-doped BiCuSeO [(a)–(c)], $Bi_{0.9}CuSeO$ [(d)–(f)], and $BiCuSe_{0.9}O$ [(g)–(i)] samples. The Gaussian fitting curves for each oxidation state are also shown for each spectrum.

using a standard defect theory. A further discussion of the chemical shift is expected to fully understand the changes of the valence state and carrier number in this oxide thermoelectric compound.

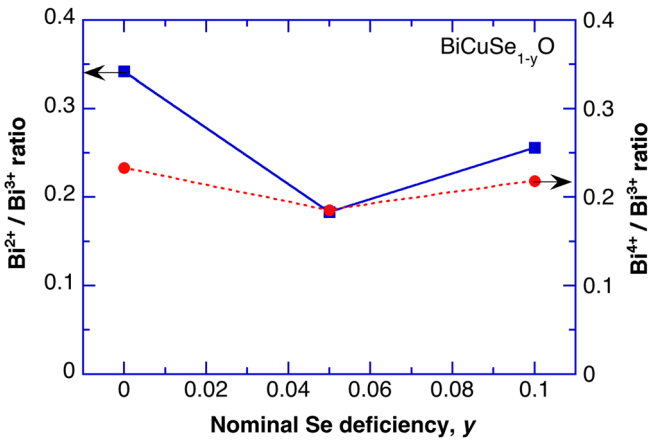

FIG. 11. The ratios of Bi^{2+}/Bi^{3+} and Bi^{4+}/Bi^{3+} in the XPS spectra for the $BiCuSe_{1-y}O$ samples, as a function of the Se deficiency, y, in the nominal composition.

IV. CONCLUSIONS

We have fabricated the BiCuSeO bulks using raw materials with Bi or Se deficiencies in the starting composition and investigated crystallographic properties, chemical composition, and oxidation state of each element and thermoelectric properties. The important results and conclusions obtained from this study are summarized as follows.

(1) Owing to the Bi or Se deficiencies in the starting composition, excessive raw materials and related compounds were deposited as impurity phases. However, the matrix phase is nearly the stoichiometric BiCuSeO phase. These results are in clear contrast with the previous reports of the $BiCu_{1-x}SeO$ samples fabricated by Cu deficiencies in the starting composition.

(2) For $Bi_{1-x}CuSeO$ samples, the electrical resistivity, $\rho(T)$, decreases and thermoelectric power, $S(T)$, also decreases with increasing the contents of Bi deficiencies in the starting composition in spite of nearly the stoichiometric matrix phase.

(3) On the other hand, for $BiCuSe_{1-y}O$ samples, the $\rho(T)$ value decreased for the y value up to 0.05 and then slightly increased for the $y = 0.1$ sample, and the $\rho(T)$

value at high temperatures is independent of the y value. The $S(T)$ value changes closely depending on the $\rho(T)$ value.

(4) Using the XPS measurements, the actual oxidation states of Bi and Cu deviate from the formal valences of stoichiometric $Bi^{3+}Cu^{1+}Se^{2-}O^{2-}$. Based on the standard defect theory, in the $Bi_{1-x}CuSeO$ system, the hole carriers originating from the Bi vacancies are introduced into conductive $[Cu_2Se_2]^{2-}$ layers and then, the electrical resistivity decreases with increasing x. In the $BiCuSe_{1-y}O$ system, the Bi^{2+}/Bi^{3+} and Bi^{4+}/Bi^{3+} ratios in the XPS spectra took a minimum for the $y = 0.05$ sample and then increase for the $y = 0.1$ sample. These y dependences show a similar trend to the electrical resistivity and the hole concentration. We proposed charge valance equations and the origin of the carriers in the present BiCuSeO samples.

(5) The maximum thermoelectric dimensionless figure of merit, $ZT = 0.60$, was achieved at 773 K for the $Bi_{1-x}CuSeO$ samples ($x = 0.025$ and 0.05). These results are in clear contrast with the reported results for the Cu deficiency bulks.

ACKNOWLEDGMENTS

This work was performed under the Inter-university Cooperative Research Program of the Institute for Materials Research, Tohoku University (Nos. 15K0119, 16K0039, and 17K0065). The authors thank Dr. K. Nonaka, Mr. T. Itoh, Mr. K. Sasaki, and Mr. K. Kobayashi of Iwate University for their technical supports of EPMA, SEM, and XPS measurements.

[1]A. M. Kusainova, P. S. Berdonosov, L. G. Akselrud, L. N. Kholodkovskaya, V. A. Dolgikh, and B. A. Popovkin, J. Solid State Chem. **112**, 189 (1994).
[2]Y. Kamihara, H. Hiramatsu, M. Hirano, R. Kawamura, H. Yanagi, T. Kamiya, and H. Hosono, J. Am. Chem. Soc. **128**, 10012 (2006).
[3]Y. Kamihara, T. Watanabe, M. Hirano, and H. Hosono, J. Am. Chem. Soc. **130**, 3296 (2008).
[4]M. Palazzi and S. Jaulmes, Acta Crystallogr., Sect. B **37**, 1337 (1981).
[5]P. S. Berdonosov, A. M. Kusainova, L. N. Kholodkovskaya, V. A. Dolgikh, L. G. Akselrud, and B. A. Popovkin, J. Solid State Chem. **118**, 74 (1981).
[6]C. Barreteau, D. Bérardan, E. Amzallag, L.-D. Zhao, and N. Dragoe, Chem. Mater. **24**, 3168 (2012).
[7]H. Hiramatsu, H. Yanagi, T. Kamiya, K. Ueda, M. Hirano, and H. Hosono, Chem. Mater. **20**, 326 (2008).
[8]L.-D. Zhao, D. Berardan, Y. L. Pei, C. Byl, L. Pinsard-Gaudart, and N. Dragoe, Appl. Phys. Lett. **97**, 092118 (2010).
[9]J. Li, J. Sui, Y. Pei, C. Barreteau, D. Berardan, N. Dragoe, W. Cai, J. He, and L.-D. Zhao, Energy Environ. Sci. **5**, 8543 (2012).
[10]J. P. Heremans, V. Jovovic, E. S. Toberer, A. Saramat, K. Kurosaki, A. Charoenphakdee, S. Yamanaka, and G. J. Snyder, Science **321**, 554 (2008).
[11]T. C. Harman, P. J. Taylor, M. P. Walsh, and B. E. LaForge, Science **297**, 2229 (2002).
[12]J. P. Heremans, C. M. Thrush, and D. T. Morelli, Phys. Rev. B **70**, 115334 (2004).
[13]Y.-L. Pei, J. He, J.-F. Li, F. Li, Q. Liu, W. Pan, C. Barreteau, D. Berardan, N. Dragoe, and L.-D. Zhao, NPG Asia Mater. **5**, e47 (2013).
[14]L. Pan, D. Bérardan, L. Zhao, C. Barreteau, and N. Dragoe, Appl. Phys. Lett. **102**, 023902 (2013).
[15]J. Sui, J. Li, J. He, Y.-L. Pei, D. Berardan, H. Wu, N. Dragoe, W. Cai, and L.-D. Zhao, Energy Environ. Sci. **6**, 2916 (2013).
[16]S. Ohta, T. Nomura, H. Ohta, M. Hirano, H. Hosono, and K. Koumoto, Appl. Phys. Lett. **87**, 092108 (2005).
[17]M. Ohtaki, T. Tsubota, K. Eguchi, and H. Arai, J. Appl. Phys. **79**, 1816 (1996).
[18]D. Berardan, E. Guilmeau, A. Maignan, and B. Raveau, Solid State Commun. **146**, 97 (2008).
[19]Y. Liu, L.-D. Zhao, Y. Liu, J. Lan, W. Xu, F. Li, B.-P. Zhang, D. Berardan, N. Dragoe, Y.-H. Lin, C.-W. Nan, J.-F. Li, and H. Zhu, J. Am. Chem. Soc. **133**, 20112 (2011).
[20]H. Zhu, T. Su, H. Li, C. Pu, D. Zhou, P. Zhu, and X. Wang, J. Eur. Ceram. Soc. **37**, 1541 (2017).
[21]Y. Goto, M. Tanaki, Y. Okusa, T. Shibuya, K. Yasuoka, M. Matoba, and Y. Kamihara, Appl. Phys. Lett. **105**, 022104 (2014).
[22]H. Hiramatsu, T. Kamiya, T. Tohei, E. Ikenaga, T. Mizoguchi, Y. Ikuhara, K. Kobayashi, and H. Hosono, J. Am. Chem. Soc. **132**, 15060 (2010).
[23]A. Zakutayev, J. Tate, and G. Schneider, Phys. Rev. B **82**, 195204 (2010).
[24]F. Izumi and T. Ikeda, Mater. Sci. Forum **321–324**, 198–203 (2000).
[25]*Practical Surfaces Analysis*, 2nd ed., edited by D. Briggs and M. P. Seah (John Willey & Sons, New York, 1993), Vol. 1.
[26]C.-L. Hsiao and X. Qi, Acta Mater. **102**, 88–96 (2016).
[27]L. D. Zhao, J. Q. He, D. Berardan, Y. H. Lin, J. F. Li, C. W. Nan, and N. Dragoe, Energy Environ. Sci. **7**, 2900–2924 (2014).
[28]S.-H. Wei, Comput. Mater. Sci. **30**, 337–348 (2004).
[29]S.-H. Wei and S. B. Zhang, Phys. Rev. B **66**, 155211 (2002).